UNIVERSITY OF COLORADO BOULDER

Classical Analysis of High Harmonic Generation

by

Benjamin Kurt Miller

A thesis submitted in partial fulfillment for
Departmental Honors in Physics

Thesis Adviser:
Dr. Agnieszka Jaron-Becker, JILA and Department of Physics

Defense Committee Members:
Dr. Agnieszka Jaron-Becker, JILA and Dept. of Physics
Dr. Andreas Becker, JILA and Dept. of Physics
Dr. James Thompson, JILA and Dept. of Physics, Honors Council representative
Dr. Daniel Jones, HRAP and Honors LEAD Neighborhood

defended on

November 5th, 2015

UNIVERSITY OF COLORADO BOULDER

Abstract

Department of Physics

Classical Analysis of High Harmonic Generation

by Benjamin Kurt Miller

When bound electrons are exposed to high intensity, near-infrared light they radiate at integer multiples of the driving field's frequency. The emitted light can reach into the extreme ultraviolet and soft x-ray region of the electromagnetic spectrum. Since the emitted frequencies are high and confined to integer multiples of the driving field's frequency, this process is called High Harmonic Generation.

The accepted semi-classical model for this process, given a linearly polarized driving field, was developed by P. B. Corkum. It is called the "Three Step Model" and it divides High Harmonic Generation by three major events: ionization, acceleration, and recombination. The model was expanded to $\omega - 2\omega$ non-linear field mixing by Milosevic et al. but the new model requires a long tunnel exit with a non-zero exit velocity. The values of momentum and time are saddle points for the quasi-classical action at the time of ionization and recombination. These saddle points could be used for calculating the spectrum of HHG, they are connected with critical times in the Three Step Model; and, in this thesis, they are used to determine potential electron trajectories.

In this thesis I calculated saddle points, electric fields, quiver radii: α, ponderomotive energies: U_p, and electron trajectories for a selection of driving fields. I varied the ratio of intensities in $\omega - 2\omega$ field mixing, and calculated maximum classically predicted harmonics for each combination.

Acknowledgements

The funding for this project was generously provided by UROP at the University of Colorado Boulder, NSF PFC Grant #1125844, and Federal Work Study.

The project would not have been possible without the help of the members of the Ultrafast AMO Theory group Michelle Miller, Andrew Spott, Cory Goldsmith, Yuqing Xia, Ran Brynn Reiff, and Zhi-Chao Li. These people helped me learn the process of theoretical research. They were a great audience to present the research to. I really enjoyed working with all of you!

Thank you to my family for supporting me while I was working on this project.

Most of all, I'd like to thank my advisers Agnieszka Jaron-Becker and Andreas Becker. The two of them guided my pursuit of this project with brilliance, humor, and grace.

Contents

List of Figures

Chapter 1

Introduction

When bound electrons are exposed to high intensity, near-infrared light they radiate at integer multiples of the driving field's frequency. The emitted light can reach into the extreme ultraviolet and soft x-ray region of the electromagnetic spectrum. Since the emitted frequencies are high and confined to integer multiples of the driving field's frequency, this process is called High Harmonic Generation (HHG). Semi-classical models for HHG were a new topic of theoretical interest in the 1990s and early 2000s. The first triumph of semi-classical trajectories was demonstrated by Corkum in 1993. He applied the Three Step Model which provided a semi-classical explanation for the cutoff frequency and an intuitive explanation for the laser light's effect on HHG [1]. The concept was extended to more complicated polarizations of light by Milosevic in 2000. Milosevic introduced a long tunnel exit for polarizations involving $\omega - 2\omega$ field mixing. This new technique allowed for electron trajectories that return to the nucleus of the parent ion, a necessary quality for a trajectory to lead to high harmonics [2].

The focus of the research for this thesis was to calculate electron trajectories for a variety of polarizations. Interest in these trajectories was renewed because experimentalists want to generate high harmonics using non-linear polarizations. Insight into the semi-classical picture might be useful for creating better experiments. There are also a few open questions of theoretical interest: Is it possible to draw any conclusions about the nature of a harmonic from the shape of the trajectory? Can we connect the probability of a trajectory to any semi-classical parameters in the calculation? At what length does the tunnel exit become improbable enough that it is ignorable?

This chapter is designed as an introduction and review of the necessary components to understand the research. The topics covered include a short review of electromagnetic radiation, an introduction to strong field effects, and an overview of the interest in High-Order Harmonic Generation.

Before getting to the effects of the strong field we review the properties of electromagnetic radiation related to this thesis.

1.1 Review of Electromagnetic Radiation

Electromagnetic radiation (EMR) is a form of energy that is released in certain electromagnetic processes. The processes that are most relevant to this thesis include the time varying electric dipole moment and electron transitions between atomic energy levels. EMR interacts differently depending on the frequency of its oscillations, or put a different way, the energy of the constituent photons. EMR is a highly prevalent phenomenon, for example, an important type of EMR is visible light! [3]. EMR and light will be used interchangeably in this thesis. When referring to a particular frequency band of light, the name of the frequency band will be mentioned explicitly.

EMR can be treated both classically and quantum mechanically. Both descriptions are necessary for modeling HHG, so both will be used throughout the thesis. Classically, EMR consists of electromagnetic waves which propagate at the speed of light through a vacuum. These waves have a frequency and wavelength that determines their behavior. Quantum mechanically, EMR consists of photons which are massless particles that carry energy, momentum, and angular momentum. Each photon has a quantum of energy associated to it based on its frequency.

1.1.1 Wave-particle Duality

In the previous section EMR was treated in two different ways: classically and quantum mechanically. This property is explained by light's wave-particle duality. The discovery of light's dual nature is amongst the most important achievements of physics [4].

The experimental evidence of light acting like a wave was available before confirmation of its particle nature. Light interferes with itself, diffracts, and polarizes. These processes are characteristic behaviors of waves, not particles. However, other processes, including the photoelectric effect, could not be explained using just a wave theory of light. The modern theory of light includes both of these representations of light because light is both a wave and a particle [5].

Polarization and quanta of light, photons, are discussed explicitly below because they are relevant to the research presented in this thesis.

1.1.2 Polarization

Transverse waves in three dimensions must be polarized because they can oscillate in more than one direction. The polarization determines the orientation of the oscillation in space. The polarization direction of EMR is defined by the direction of oscillation of the electric field. Any polarization in three dimensions can be created by linear combinations of two orthogonal electric field vectors. Consider Fig. 1.1 for polarizations generated by orthogonal electric field vectors, and Fig. 1.2 for a more detailed description of circular polarization.

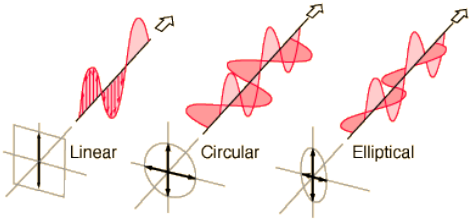

FIGURE 1.1: Polarization examples. The non-linear polarizations are a superposition of out of phase orthogonal linear electric fields [5].

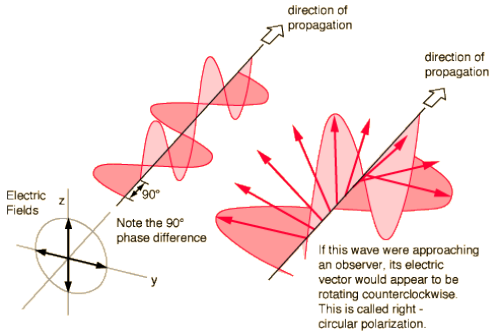

FIGURE 1.2: Circular polarization require the orthogonal electric fields to be 90° out of phase. The figure clarifies the handedness for this polarization [5].

An example of an elliptically polarized electric field vector is:

$$\mathbf{E}(t) = \frac{1}{i}\left[\frac{E_0}{\sqrt{1+\epsilon^2}}(\hat{\mathbf{e}}_1 - i\epsilon\hat{\mathbf{e}}_2)e^{i\omega t}\right] + \text{c.c.} \tag{1.1}$$

where ϵ $(-1 \leq \epsilon \leq 1)$ and E_0 are the ellipticity and the electric field vector amplitude, respectively, and $\hat{\mathbf{e}}_1$ and $\hat{\mathbf{e}}_2$ are two orthogonal real unit vectors. $|\epsilon| \geq 0$ implies an elliptical field with the limit $|\epsilon| = 1$ meaning circular and $|\epsilon| = 0$ meaning linear. "c.c." denotes adding the complex conjugate. It is simple to write the electric field for $\omega - 2\omega$ field mixing by using the superposition of another elliptical polarization with angular frequency 2ω. The general equation for electric field polarization used in this thesis is bichromatic $(\omega - 2\omega)$ and circularly polarized. Starting with the general equation for two color field mixing for elliptical polarizations

$$\mathbf{E}(t) = \frac{1}{2i}\left[\frac{E_1}{\sqrt{1+\epsilon_1^2}}(\hat{\mathbf{e}}_1 - i\epsilon_1\hat{\mathbf{e}}_2)e^{i\omega t} + \frac{E_2}{\sqrt{1+\epsilon_2^2}}(\hat{\mathbf{e}}_1 - i\epsilon_2\hat{\mathbf{e}}_2)e^{2i\omega t}\right] + \text{c.c.} \tag{1.2}$$

and limiting $\epsilon_1 = \epsilon_2 = 1$ or $\epsilon_1 = \epsilon_2 = -1$ we define two corotating or two counter-rotating circularly polarized fields. The net polarization can be significantly altered by varying the intensity ratio of the source. When considering a particular intensity ratio, the net polarization will be shown by means of a parametric plot of the electric field vector in time.

1.1.3 Quanta of Light: Photons

Photons are elementary particles that have zero rest mass and carry the energy, momentum, and angular momentum of light. The important concept for this thesis is the quantized energy of a photon. The energy of a photon is directly related to its frequency, given by $E = \hbar\omega$, where ω is the angular frequency of the photon and $\hbar$ is the reduced Planck's constant. Notice, if photon A has twice the energy of photon B, then photon A is twice the frequency of photon B. That means that photon A is the second harmonic of photon B. This concept will return while covering the quantum description of HHG.

1.1.4 Extreme Ultraviolet and Soft X-Ray Attosecond Pulses

An exciting effect from high-order harmonic generation is the generation of extreme ultraviolet (XUV) and soft x-ray pulses on the order of attosecond duration. (1 as $= 10^{-18}$ s). The high frequency spectral region from linear polarization driven HHG forms a comb of harmonics with similar intensities which also exhibit a smooth spectral phase distribution. This kind of frequency distribution is ideal for synthesis of ultrashort pulses. If one selects for the highest harmonics, the radiation takes the form of a train of ultrashort XUV pulses, with typical durations of hundreds of attoseconds which are generated regularly at every half of the driving field's period [6]. High-order harmonic methods for ultrashort pulse generation do not achieve the Fourier limit (i.e. a band of frequencies with constant relative phase) because these attosecond pulses exhibit chirped behavior called the "atto-chirp." An explanation for the cause of the atto-chirp in linear polarization driven HHG is provided using the Three Step Model in Sec. 2.4. These

attosecond pulses have proven useful for the time resolution of ultrafast (attosecond) dynamics [7].

1.2 Strong Field Effects

The study of intense light begins with the invention of the laser in 1960. Lasers differ from other light sources because they produce coherent light. Coherent light from a laser can be tightly focused and can reach intensities that are impossible using other light sources. The laser can be tuned to a particular frequency so that it produces monochromatic light which is made up of a very narrow band of frequencies. Lasers are the source required for generating high intensity light beams that drive HHG and other strong field effects.

These processes require non-linear strong field ionization, thus they occur when $\hbar\omega_0 < |E_0|$. Where $|E_0|$, also known as the ionization potential, is the magnitude of the energy required to extract the most energetic bound electron from the system. ω_0 is the frequency of the incident radiation. Non-linear ionization requires multiple photon interactions because several photons must be absorbed before the bound electron's energy is higher than the ionization potential. Multiphoton processes are justified by the energy time uncertainty principle, $\delta\omega\delta t \geq \hbar$, which allow the system to pass through virtual states for δt given an energy uncertainty of $\delta\omega$ [7].

Intense laser fields have introduced several effects that are not predicted by perturbation theory. These effects are referred to as "Strong Field Effects" because they were discovered with the advent of very intense fields in laboratory settings. The different effects include: Above Threshold Ionization (ATI), Double Ionization, and HHG. ATI and Double Ionization will only be covered briefly, but references will be provided to learn more about the subjects.

Above Threshold Ionization occurs when an electron absorbs many more photons than necessary for ionization so the electron is ionized with high kinetic energy. Above Threshold Ionization was first reported by Pierre Agostini et al. in 1979 [8].

Double Ionization can be sequential or non-sequential. Sequential double ionization occurs when one electron is ionized, then another after it. In non-sequential double ionization both electrons leave the system at the same time. In rare gas atoms, non-sequential double ionization was observed by L'Huillier et al [9].

The final effect is HHG which will be covered in greater detail in Chapter 2. These processes require understanding strong field ionization which is explained below.

1.2.1 Tunneling Ionization

We consider an electron in the ground state of a hydrogen atom. The electron is strongly bound by the Coulomb potential. When the potential well interacts with a strong linearly polarized electric field from a laser, the net potential is tilted allowing the electron to tunnel out into the continuum. (Fig. 1.3). The tunneling must occur before the electric field has a chance to change direction again. We introduce the Keldysh adiabaticity parameter γ to determine whether tunneling ionization is possible.

$$\gamma = \omega_0 = \sqrt{\frac{|E_0|}{2U_p}} \tag{1.3}$$

Where U_p is the ponderomotive energy given by $U_p = e^2 \langle \mathbf{A}^2(t) \rangle / 2m$, and $|E_0|$, also known as the ionization potential, is the magnitude of the energy required to extract the most energetic bound electron from the system. When $\gamma < 1$ the approximate tunneling time is considered to be much less than a period of the driving field. For fields that fulfill this condition, we can approximate the electric field as constant during tunneling [7].

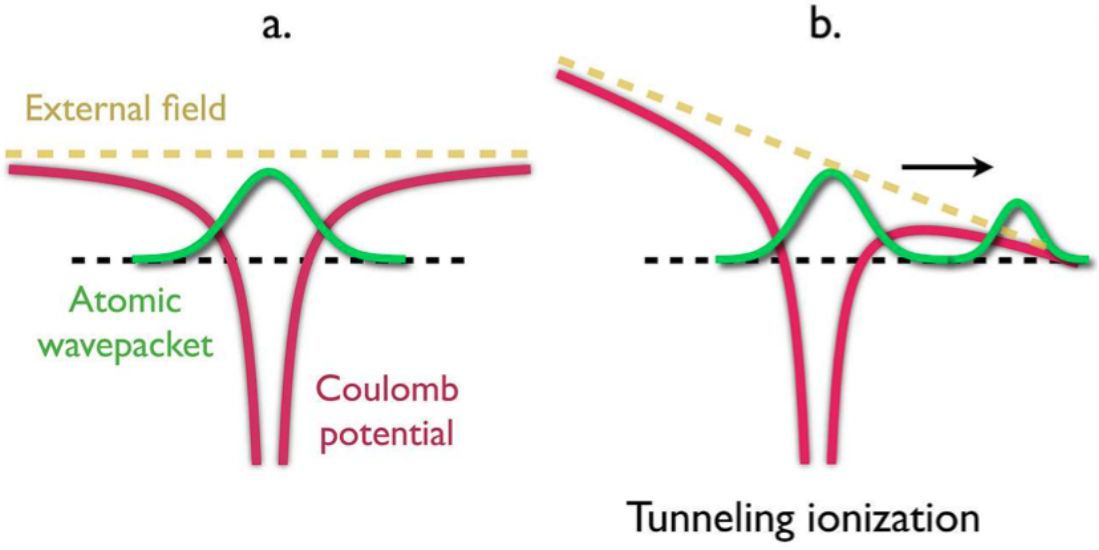

FIGURE 1.3: a. Electron in its bound state. b. System exposed to strong field, electron tunneling is possible [7].

1.2.2 Multiphoton Ionization

Multiphoton ionization (MPI) dominates when $\gamma >> 1$, meaning the ionization potential is greater than the ponderomotive energy, which happens for relatively high frequencies or weak fields. Two sets of multiphoton interactions are shown in Fig. 1.4 and Fig. 1.5,

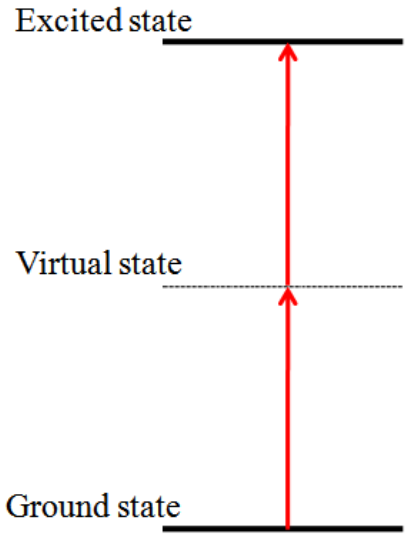

FIGURE 1.4: Two low frequency photons interact with an electron exciting it to a higher energy bound state. Notice the electron passes through a virtual state.

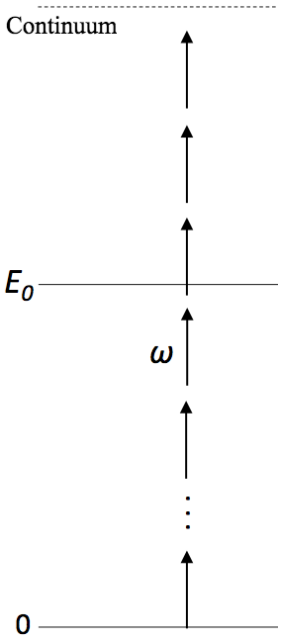

FIGURE 1.5: Many low frequency photons interact with an electron to ionize it.

recall multiphoton interactions are justified by virtual states. If the number of photons multiplied by the energy of each photon is greater than the ionization potential the electron is freed. Given a low intensity field, electrons enter the continuum with the minimum number of photons required to free the electron. As a result, the electrons leave with a very low amount of kinetic energy– less than the energy of a single photon. These conditions are known as the perturbative regime. If the field becomes intense enough, this model breaks down because electrons are ionized with many more photons than the minimum required. When the fields are intense strong field effects become significant such as ATI and HHG. The first experiments on multiphoton ionization were performed in 1977 by Lompre et al [10].

Chapter 2

High-Order Harmonic Generation

When matter interacts with very intense light the non-linear response can not be explained using perturbation theory. The electrons in the exposed sample radiate at the driving field's frequency and also at frequencies that are not contained within the driving field. If the sample is exposed for many cycles, interference leads to radiation at integer multiples of the driving field's frequency. These emissions are known as harmonics and the most energetic harmonics can extend as far as the soft x-ray regime. The process is called High Harmonic Generation (HHG). HHG produces high photon energies and the wide range of frequencies. Observe this behavior in the HHG spectrum given a linearly polarized driving field in Fig. 2.1. The spectrum is a plot that characterizes radiation and shows intensity versus frequency. For HHG, we expect to find a perturbative region with a negative slope for lower frequencies, a plateau where all harmonics are odd and generated with similar intensities, and a sharp cut-off where harmonic generation stops.

This thesis focuses on the microscopic scale description– just one atom is assumed to be exposed to intense light. Modeling the system with Strong Field Approximation (SFA) determines information about the energy spectrum of the harmonics released. This quantum mechanical calculation reveals interesting information, but one cannot glean much physical intuition in this model. The content of this thesis is a search for physical intuition about these systems by means of semi-classical analysis.

High Harmonic Generation produces coherent light in high frequency regions of electromagnetic spectrum higher than any laser currently available. Calculating and explaining High Harmonic Generation requires quantum mechanics. We can learn about the dipole and the HHG spectrum by performing quantum mechanical calculations. Semi-classical calculations reveal information about trajectories and provide physical intuition.

In this chapter we will provide a brief description of the important features of HHG then motivate the study of HHG, particularly non-linear polarizations. We will present two different models of HHG: the quantum multiphoton absorption model and the semi-classical tunneling ionization model known as the Three Step Model. The two approaches presented below can be thought of as two sides to the same coin. Both explanations describe the same process, but one might be better suited to understand HHG depending on the situation.

2.1 Important Features of HHG

The HHG spectrum generated by a linearly polarized driving field has the important features presented in Fig. 2.1. At low harmonic frequencies, perturbative effects dominate and the intensity has a negative slope. The non-perturbative plateau region follows. In the spectrum, only odd harmonics are generated for systems with inversion symmetry such as atoms. This occurs because harmonics appear in bursts when the driving field is approaching a zero crossing, so the bursts occur at twice the driving field's frequency. These bursts can be modeled by a Dirac delta comb which has a Fourier transform of only odd harmonic frequencies [11]. ω_{max} marks the cut-off frequency, which can be determined using Eqn. 2.1 first explained semi-classically for linear polarizations by Corkum in 1993 [1].

$$\hbar\omega_{max} = |E_0| + 3.17U_p \tag{2.1}$$

E_0 is the depth of the energy well binding the electron, also known as the Ionization Potential. U_p is the ponderomotive energy which is the time averaged energy of an electron exposed to the driving field alone. $U_p = e^2 \left\langle \mathbf{A}^2(t) \right\rangle / 2m$. $|e| = e$ is the absolute value of the charge of the electron, $\mathbf{A}(t)$ is the vector potential, and m is the mass of the electron. Most examples studied in this thesis are generated by 800 nm driving fields at $10^{14} \frac{W}{cm^2}$. This light is in the near infrared and can be reliably generated by the Titanium-Sapphire Laser at high intensity. The intensity is kept below $10^{15} \frac{W}{cm^2}$ because relativistic effects and the effect of the magnetic field on the electron's motion play a significant role above such intensities.

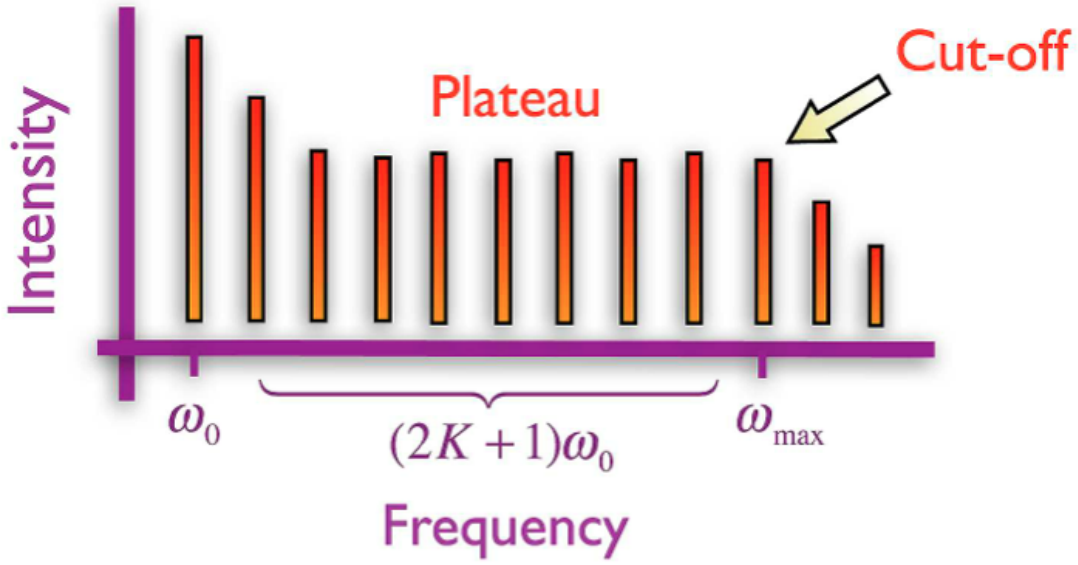

FIGURE 2.1: Model spectrum for HHG given a linearly polarized driving field. The perturbative regime includes lower harmonics and has a negative slope. The non-perturbative plateau and cut-off harmonics are odd. The harmonics sharply decrease in intensity after the cut-off [7].

2.2 Motivation for HHG

High-Order High Harmonic Generation helped extend coherent radiation to higher frequencies than ever before; however, there are other interesting and useful properties of HHG. To help motivate a particularly important application of HHG, generation of attosecond pulses, let's turn our attention to a question from the former governor of California, Leland Stanford.

Stanford wanted to know if, at any point during its gallop, a horse had all of its feet in the air. The answer to this question cannot be determined with certainty using only the human eye. Stanford needed the help of something that could take multiple pictures in the time it took a horse to complete one period of its gallop. A photographer, Eadweard Muybridge, had just what he needed. Muybridge arranged for many threads to be setup along a racetrack and each thread was connected to a camera which took a picture when the thread was pulled or broken. The horse ran along the track and each picture was snapped during a different section of the horse's gallop. In this way Muybridge solved the mystery by time resolving the horse's motion.

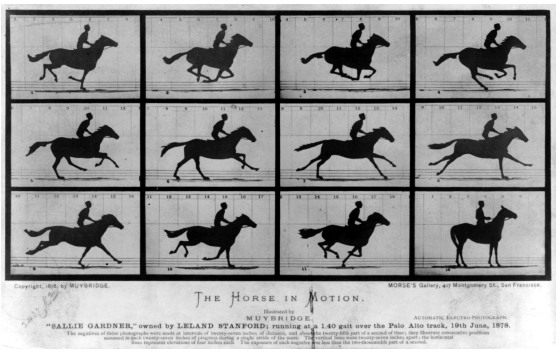

FIGURE 2.2: Eadweard Muybridge photographed a horse in motion to answer Stanford's riddle [12].

Attosecond pulses (atto- = 10^{-18}), generated by HHG, are similar to the cameras in this example. The only way to time resolve processes that happen very quickly is by taking many "pictures" during the process. Attosecond pulses provide a "camera" on the timescale required to image electron dynamics. Attosecond pulse generation is made possible by HHG because of the wide plateau and the phase locking characteristics of the harmonics. The plateau offers a wide selection of frequencies in frequency space. Taking a Fourier Transform translates into a narrow time band: an attosecond pulse. Creating a short pulse requires coherence in the frequencies selected. Luckily HHG provides phase locking of the harmonics [7].

The experimental interest in HHG is shifting towards high intensity elliptically polarized pulses. An example of such interest is described in Ref [13]. Circularly Polarized X-Rays can be used to determine some magnetic properties of a material. This process involves looking at the difference in absorption spectra from two exposures to circularly polarized x-ray radiation. In each exposure, the direction of polarization changes from left to right circularly polarized, or vice-versa. By comparing the absorption spectra

we can learn about the the magnetic material's spin or magnetic moment. Another property of circularly polarized high harmonics are their ability to detect and analyze chiral molecules. If we compare two absorption spectra with differently rotating circular polarizations and notice a difference in absorption the molecules are chiral. An overview of chirality can be found in Ref. [14] and more information about these techniques can be found in Ref. [15].

2.3 Quantum Description of High Harmonic Generation

The quantum picture of HHG relies on multiphoton ionization and assumes that many low energy photons are absorbed by a ground state electron, then all of that energy is released as a high energy photon (See Fig. 2.3). Since photons can only be absorbed by an electron in integer multiples, the high energy photon is always an integer multiple of low energy photons. The integer relation is the reason each high energy photon is called a high harmonic. Quantum High Harmonic Generation occurs in the strong field

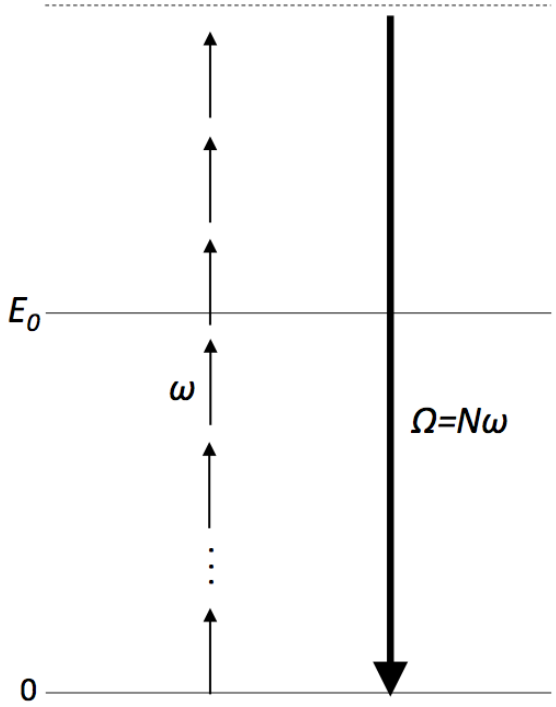

FIGURE 2.3: N photons of frequency ω are absorbed by an electron in its ground state. One photon of frequency $N\omega$ is emitted as a high harmonic.

because many more photons are absorbed than necessary to send the electron to the continuum. Characterizing the behavior of the system requires calculating the time dependent electric dipole moment of the electron in the field. This process is presented for linear polarizations by M. Lewenstein et al. in Ref. [16] and for elliptical polarizations by D. B. Milosevic et al. in Ref. [2].

Qualitatively, the first step is to take the inner product of the time dependent wavefunction of the whole system with the electric dipole operator acting on the same wavefunction. The evolution of the wavefunction in the presence of the intense electric field is far too complicated to make this calculation, so we have to approximate it using the Strong Field Approximation (SFA). In this approximation, the wavefunction is divided into three contributing factors related to the following states of the process: the bound electron siting in the ground state before interaction, the electron oscillating in the continuum under the influence of the laser field alone after it has been freed, and the electron bound in the ground state again after the interaction. When the electron is in the continuum under the influence of the laser field the Coulomb potential is neglected.

This approximation is a step towards calculating the electric dipole moment, but another approximation must be made. In order to calculate the electric dipole moment using SFA, the quasi-classical action must be calculated.

$$S(\mathbf{q}, t_i, t_f) = \int_{t_f}^{\infty} (E_0 + n\hbar\omega)dt + \frac{1}{2m}\int_{t_i}^{t_f} dt[\hbar\mathbf{q} + e\mathbf{A}(t)]^2 + \int_{-\infty}^{t_i} dtE_0 \tag{2.2}$$

Where E_0 is the ground state energy, n is the harmonic number, ω is the frequency of the driving field, $\hbar\mathbf{q}$ is the canonical momentum, $|e| = e$ the absoulte value of the charge of the electron, $\mathbf{A}(t)$ is the vector potential. To approximate the integral we use the complex Saddle Point Method (SPM). SPM is also called the Method of Steepest Descent. Essentially, the integral can be calculated by summing over its saddle points, shifting the complexity from solving the integral to finding the saddle points. Searching for these saddle points was a significant portion of this project and will be covered in detail in Sec. 3.2.1. Learn more about SPM in Ref. [17, 18].

2.4 Semi-Classical Description of High Harmonic Generation

The Three Step Model, introduced by Corkum for linear polarizations in Ref. [1], is a semi-classical formulation of HHG that predicts the cut-off frequency, chirped behavior of the generated harmonics, and trajectories associated with the electron's path after entering the continuum. Milosevic et al. expanded the model to include $\omega - 2\omega$ field mixing for elliptical polarizations. Milosevic's model differs from Corkum's model because a harmonic emitted electron enters the continuum away from the origin, at a point called the "tunnel exit," then follows a trajectory back to the origin.

The Three Step Model, or Simpleman's Model, divides HHG into a series of steps. At first the electron is bound to a parent atom by the Coulomb potential. Then a strong

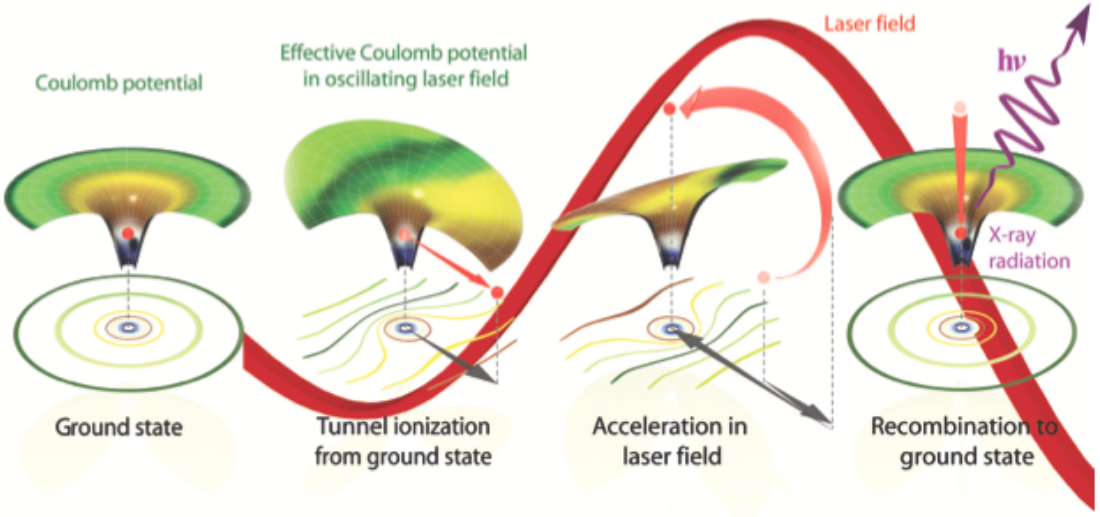

FIGURE 2.4: Three step model of HHG. This semi-classical model explained the cut-off and chirp of HHG. [19]

electric field is introduced by the laser. Since the field is strong it can distort the potential well allowing tunnel ionization. The electron enters the continuum at the origin with no velocity, but it is accelerated by the strong field. The Coulomb potential is not a short range potential, but it is assumed that the electron has enough energy that it won't be trapped by the well, and the Coulomb potential is neglected. The electron traces a path in space called a trajectory. After the electron is tunnel ionized, the electron is accelerated by the field and might cross the origin again and return to the nucleus. If this happens, the trajectory is called "closed" and the trajectory leads to high harmonic emission. When the electron returns to the nucleus with a non-zero kinetic energy, the electron's energy drops down to the ground state, releasing the energy as a high harmonic photon. This step is known as "recombination." Fig. 2.5 shows trajectories related to the cut-off, or max harmonic, drawn as the blue trajectory. In Fig. 2.5b C. Hernandez Garcia plotted the recollision kinetic energy of the particles as a function of the recollision (green points) and ionization time (red points). The maximum recollision energy takes the well-known value, $3.17U_p$, for the trajectory represented in blue. We notice that there are two possible electron trajectories that result in the same kinetic energy at recollision which means there are two possible paths for the generation of the same harmonics. We name each of these trajectories as a short and long trajectory according to whether the excursion time is greater or less than 0.63 of the driving field's period. In Fig. 2.5b we observe that the short trajectory contributions emit less energetic harmonics first followed by more energetic ones, thus imprinting a positive chirp in the harmonic radiation. This behavior is reversed for the long trajectories, which imprint a negative chirp [7].

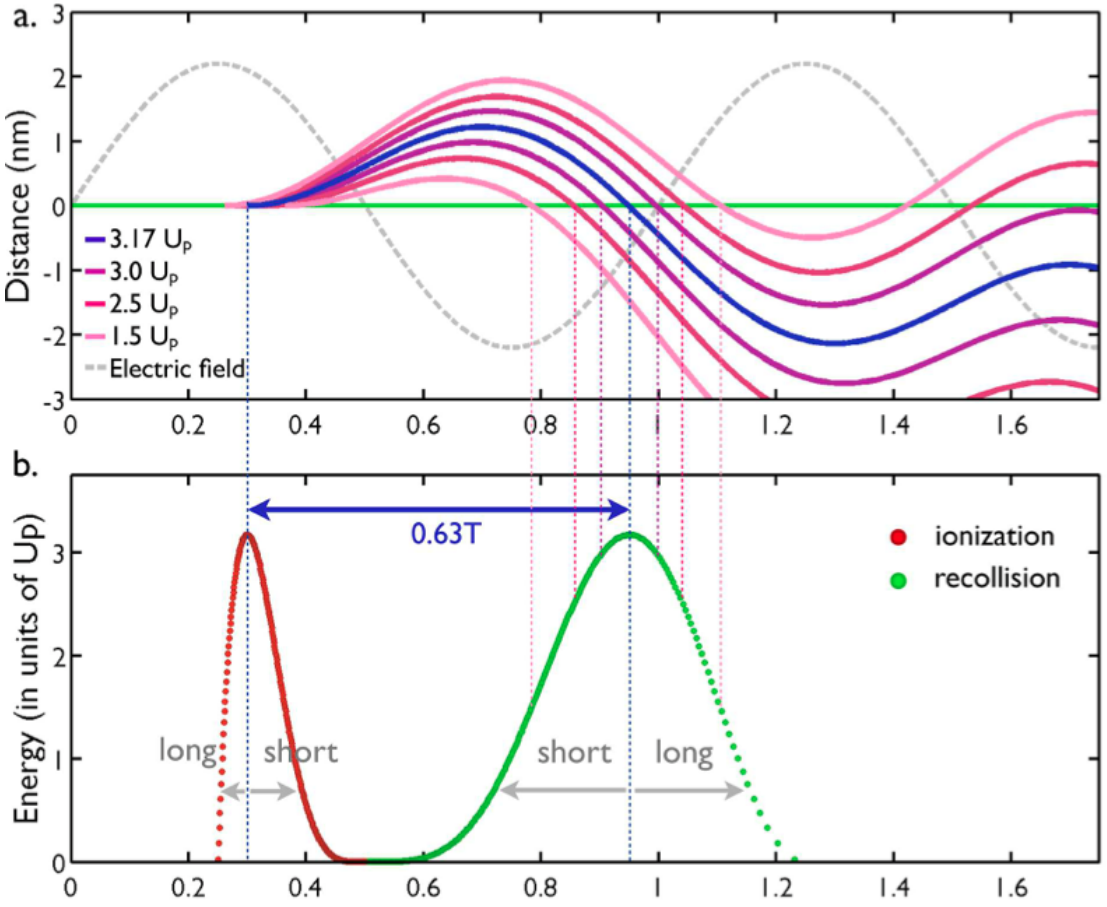

FIGURE 2.5: **a)** Sample of electronic trajectories in a monochromatic laser field of $\lambda_0 = 800$ nm and peak intensity $1.57 \times 10^{14} \frac{W}{cm^2}$. The grey-dashed line represents the electric field in arbitrary units, whereas the green line, the nucleus position. Three pairs of short and long trajectories are represented for energies at recollision of $3.0U_p$ (purple), $2.5U_p$ (dark pink) and $1.5U_p$ (light pink), whereas the most energetic trajectory, raising $3.17U_p$ at recollision, is represented in blue. The vertical axis represents the distance from the nucleus. **b)** Returning kinetic energy of the particles at the instant of the first recollision in **a.** The green points represent the recollision time, whereas the red points the ionization time. The blue arrow shows the excursion time for the most energetic trajectory, 0.63T, where T is the laser period. -C. Hernandez Garcia [7]

Generalizing the Three Step Model to $\omega - 2\omega$ field mixing for elliptical polarizations requires the introduction of the tunnel exit. Otherwise the process is essentially the same. When an electron enters the continuum in Milosevic's model it can appear away from the origin and with a non-zero velocity. These properties are necessary for any trajectory to be closed. We will turn our attention to the mathematics and theoretical methods for using these models to characterize HHG.

Chapter 3

Predicting HHG Semi-Classically

Calculating properties of High Harmonic Generation using the Three Step Model has some distinct advantages over calculations using quantum models. Semi-classical methods usually require less calculation time and they can be done on a home computer, rather than a supercomputer. Most of all, the Three Step Model reveals information we're interested in, i.e. trajectories, that direct interpretation of the time dependent electric dipole model cannot predict. We will first investigate linearly polarized driving fields because there is more published data regarding them and because they are easier to understand. After that, we focus on HHG driven by circularly polarized $\omega - 2\omega$ field mixing. Both the linear case and the field mixing case are divided into a methods section where we explain how we arrived at our data, and a results section where the data will be presented.

Although the constants will often be included in the equations, it is important to note that these calculations were made using atomic units.

$$\hbar = m = e = 1 \tag{3.1}$$

3.1 The Linearly Polarized Driving Field Case

The semi-classical model of HHG is driven by intense coherent EMR behaving like a wave with a certain polarization. The simplest polarization to consider is the case of linear polarization– where the electric field vector of the driving electromagnetic wave points along an axis. Since everything happens in one dimension it is easy to imagine the electron tracing its path as it is accelerated in one direction for some time then turned around to recombine with the nucleus at a later time. The trajectories from

linear polarization can be calculated numerically or analytically. We present numerical methods for calculating these trajectories and energies.

3.1.1 Methods for the Linearly Polarized Case

The goal for these calculations is to determine the emitted harmonic energy and the trajectory for the electron emitting that harmonic.

The driving field considered in these calculations is sinusoidal and at constant intensity. Consider a driving field of $\mathbf{E}(t) = E_1 \sin(\omega t)\hat{\mathbf{x}}$ where E_1 is the electric field maximum amplitude, and ω is the field's angular frequency. A free electron exposed to such a field moves according to the equations

$$\ddot{x}(t) = -\frac{eE_1}{m}\sin(\omega t) \tag{3.2}$$

$$\dot{x}(t) = \frac{eE_1}{m\omega}[\cos(\omega t) - \cos(\omega t_0)] \tag{3.3}$$

$$x(t) = \frac{eE_1}{m\omega^2}[\sin(\omega t) - \sin(\omega t_0) - \omega(t - t_0)\cos(\omega t_0)] \tag{3.4}$$

where t_0 is the ionization time. We calculated electron trajectories by computer simulation. First we generated a grid of electron ionization times for the first field cycle and programmed the electrons to follow a path as in Eqn. 3.4. Any electrons that returned to $x(t > t_0) = 0$ were considered HHG candidates. The time of the zero crossing is called the recombination time and is noted as t_f where $x(t_f) = 0$. The energy of an emitted harmonic is calculated using $\dot{x}(t_f)$ and $E_{harmonic} = |E_0| + \frac{1}{2}m\dot{x}(t_f)^2$. With these calculations we know the energies and trajectories of each HHG candidate.

3.1.2 Results for the Linearly Polarized Case

We compared our simulation data to the data from C. Hernandez Garcia [7]. We had agreement with the shape of the trajectories, the travel time for the highest harmonic, the cutoff, and the maximum energy. We simulated a system exposed to intense 800 nm light with linear polarization following the Three Step Model of HHG. We organized our plot of the energies of harmonic photons emitted from the system similarly to the method used for plotting kinetic energy at time of recollision in Fig. 2.5b. We plotted the harmonic order, n, of the emitted HHG photon in Fig. 3.1, which includes information about the kinetic energy at the time of recombination as well as the ionization potential $|E_0|$,

versus the time of ionization (red dots) or recombination (green dots). We calculated n by means of Eqn. 3.5.

$$n = (|E_0| + \frac{1}{2}m\mathbf{v}(t_f)^2)/(\hbar\omega) \tag{3.5}$$

In this case, we considered $|E_0|$ of a hydrogen atom in atomic units which corresponds to $|E_0| = 13.6eV$. Our plot agrees qualitatively and quantitatively with Fig. 2.5b including the positive and negative chirp corresponding to long and short trajectories, the excursion time for each electron, and the kinetic energy values at the time of recollision. Now that we have succeeded in reproducing the published results for the linear case we can move on to $\omega - 2\omega$ field mixing.

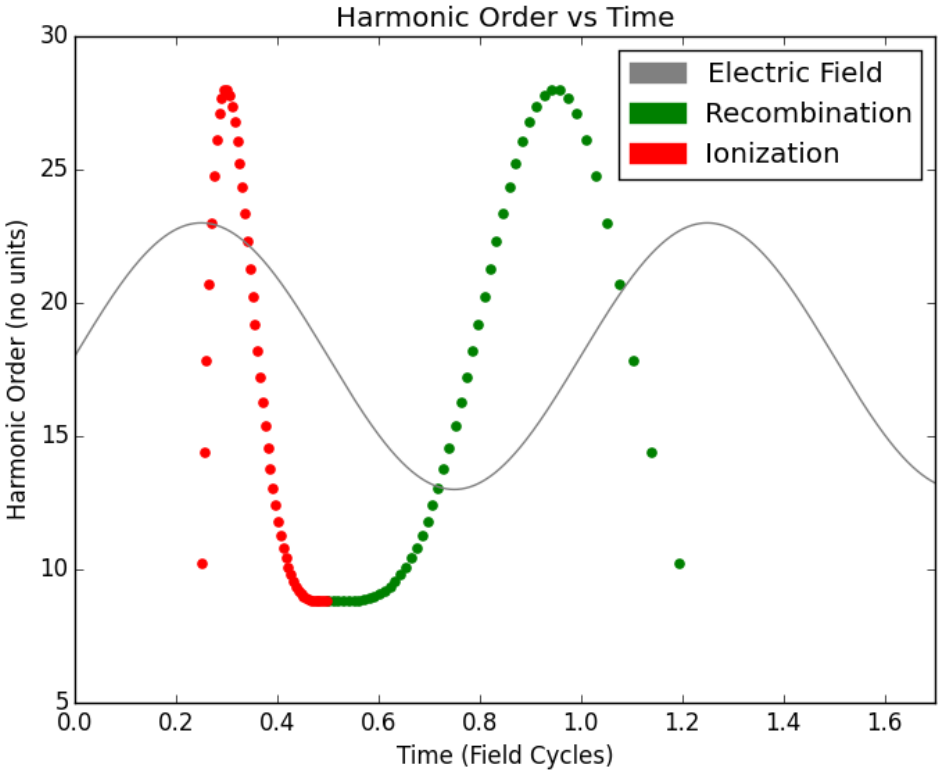

FIGURE 3.1: The energy values of harmonic photons are generated by the interaction of an electron in a driving field of 800 nm light with linear polarization. The energy of the harmonic photon emitted at recombination is plotted on the vertical axis with the green points representing recollision time and the red points representing ionization time. There is one-to-one correspondence for red and green dots meaning that every ionization dot has a recombination dot associated to it. We considered the ionization potential for Hydrogen, $|E_0| = 13.6eV$.

3.2 The Circular $\omega - 2\omega$ Field Mixing Case

The Three Step Model was quite successful for explaining the behavior of HHG given linear polarization of the driving field. When the polarization becomes non-linear things

get more complicated. In the case of $\omega - 2\omega$ field mixing, there are no closed trajectories when the electron has a tunnel exit at the origin with no initial velocity. We have to allow non-origin tunnel exits with non-zero initial velocity to find closed trajectories. The previous method of simulating the field acting on a freed electron becomes too time intensive. In two dimensions, there are 4 initial parameters (x, y, $\dot{x}$, $\dot{y}$) that must be varied before we can start simulating the electron's motion. Luckily, Milosevic et al. [2] suggests some alternative methods for finding trajectories and harmonics given $\omega - 2\omega$ field mixing.

The methods and data presented in this section represents the bulk of the research done on this project. The process of generating these trajectories was a long one that had at least one significant "dead end" along the way. For brevity, we won't explain the "dead end" methods but it is worth mentioning that the methods and results presented below represent the successful part of the search for electron trajectories.

3.2.1 Methods for Circular $\omega - 2\omega$ Field Mixing

First we introduce some important definitions which will be used throughout this section.

$$\tau = t_f - t_i \tag{3.6}$$

$$\mathbf{A}(t) = -\int^t \mathbf{E}(t')dt' \tag{3.7}$$

$$\boldsymbol{\alpha}(t) = \frac{e}{m}\int^t \mathbf{A}(t')dt' \tag{3.8}$$

$\mathbf{A}(t)$ is known as the vector potential, $\boldsymbol{\alpha}(t)$ is known as the quiver motion or quiver radius, and m is the mass of the electron. The quiver radius is the position vector of an electron accelerated by the laser field with initial conditions such that its average position is zero. These definitions hinge on the $\omega - 2\omega$ field mixing driving field we had introduced already, but is written again for reference.

$$\begin{aligned}\mathbf{E}(t) = \frac{1}{2i}\Bigg[&\frac{E_1}{\sqrt{1+\epsilon_1^2}}(\hat{\mathbf{e}}_1 - i\epsilon_1\hat{\mathbf{e}}_2)e^{i\omega t} \\ &+\frac{E_2}{\sqrt{1+\epsilon_2^2}}(\hat{\mathbf{e}}_1 - i\epsilon_2\hat{\mathbf{e}}_2)e^{2i\omega t}\Bigg] + \text{c.c.}\end{aligned} \tag{3.9}$$

This electric field represents $\omega - 2\omega$ field mixing for fields with ellipticities ϵ_1 and ϵ_2. We consider counter-rotating and corotating circularly polarized fields which are defined

by $\epsilon_1 = \epsilon_2 = 1$ or $\epsilon_1 = \epsilon_2 = -1$ respectively. The intensity I_j is related to the amplitude of the electric field E_j by $I_j = E_j^2$ in atomic units. ($I_j = \frac{1}{2}\epsilon_0 c E_j^2$ in SI units.) The ponderomotive energy for the entire field is defined by $U_p = e^2 \langle \mathbf{A}^2(t) \rangle / 2m = e^2 E_1^2/(4m\omega^2) + e^2 E_2^2/(16m\omega^2) = U_{p1} + U_{p2}$.

What follows is a brief explanation of Milosevic's et al. method from Ref. [2] to calculate electron trajectories. Recall from Sec. 2.3 we can calculate the dipole moment with the Strong Field Approximation (SFA). This process is explained in Ref. [2, 7]. Doing so yields the quasi-classical action Eqn. 2.2. As advertised, this integral can be calculated by the Saddle Point Method (SPM) which yields a system of equations 3.10 - 3.12. Solutions of this system are the saddle points necessary for calculating the quasi-classical action integral. These saddle points are directly connected with the electron trajectories.

$$\frac{m}{\tau}[\boldsymbol{\alpha}(t_f - \tau) - \boldsymbol{\alpha}(t_f) = \hbar\mathbf{q} \tag{3.10}$$

$$\frac{1}{2m}[\hbar\mathbf{q} + e\mathbf{A}(t_f - \tau)]^2 = E_0 \tag{3.11}$$

$$\frac{1}{2m}[\hbar\mathbf{q} + e\mathbf{A}(t_f)]^2 = n\hbar\omega + E_0 \tag{3.12}$$

Each equation in the system can be connected with certain conditions necessary for HHG, resulting from consiervation of energy and momentum. Eqn. 3.10 requires the electron to return to the origin, Eqn .3.11 sets the initial kinetic energy of the electron in the laser field to its energy in the atomic ground state, and Eqn. 3.12 sets the final energy of the electron equal to the energy contributions from the field plus the initial energy. Because the ground state energy of the electron is negative, solutions to this system must be complex valued. Equation 3.10 can be substituted into 3.11 and 3.12, then we have two complex equations and two complex unknowns: τ and t_f. Solutions to this system must be found numerically and finding them is not an easy process. Iterative methods require a good guess to converge and Milosevic et al. suggests a way to proceed. From their calculations $\mathrm{Im}[t_f] \approx 0$ while $\mathrm{Im}[\tau] < 0$ [2]. We follow this methods and approximate $\mathrm{Im}[t_f] = 0$ to calculate trajectories.

Before continuing we remark on imaginary time values: We cannot confidently cite a single factor that causes t_f to be real and t_i to be complex. A possible explanation might be: A tunnel exit occurs at $t = t_i = t_f - \tau$, but there is no "tunnel entrance" at t_f because we do not consider tunneling for this stage. At t_f the electron emits energy and does not travel. Since tunneling implies a non-zero outgoing probability current, then the ionization time is allowed to be complex to accommodate tunneling. Another consideration is the lack of a time operator in quantum mechanics. Consequently, Time is not an observable quantity, but rather something that must be measured by a "clock."

Having an imaginary time value at ionization doesn't correspond to the event happening at an "imaginary time" rather it serves as a parameter in our calculation. In this thesis, imaginary time is used as one of the tools to find closed trajectories. For further discussion on the topic of complex time values related to tunneling refer to Ref. [2, 20].

Armed with the assumption that $\mathrm{Im}[t_f] = 0$ we can start finding trajectories. By doing a few substitutions from our system above we arrive at just one equation:

$$\frac{1}{2m}\{\frac{m}{\tau}[\boldsymbol{\alpha}(t_f - \tau) - \boldsymbol{\alpha}(t_f)] + e\mathbf{A}(t_f - \tau)\}^2 = E_0 \tag{3.13}$$

We can solve this equation by fixing t_f and solving for complex τ. We use the iterative Newton's method for finding τ. First we create a grid of one hundred t_f values equally spaced between time of 1.05 field cycles and 1.7 field cycles. Then we create a grid of guesses for τ on a square in the complex plane with the bottom left corner at zero and with side length of one field cycle. We apply the fixed t_f and the guesses for τ to the Newton's method package contained in the library of python, SciPy, allowing 250 iterations for convergence. Any duplicates of fixed t_f and iterated τ are removed. We consider trajectories with excursion times less than one period of the driving field, because those are more likely to be physical. i.e. $\mathrm{Re}[\tau] \leq \frac{2\pi}{\omega}$.

We use the solutions of Eqn. 3.13: fixed t_f and iterated τ, to determine the trajectories and harmonics. Not every set of t_f and τ generates harmonic trajectories. Harmonics are limited to $n\omega,\ n = 0, 1, 2, ...$ therefore we have to remove the sets of t_f and τ that do not emit a harmonic at recombination. We do this by calculating the energy of emitted photons and limiting them to harmonics of the driving field like in Eqn. 3.14.

$$n\hbar\omega = |E_0| + \frac{m}{2}\{Re[\mathbf{v}(t_f)]^2 - Im[\mathbf{v}(t_f)]^2\} \tag{3.14}$$

$$m\mathbf{v}(t_f) = \frac{m}{\tau}[\boldsymbol{\alpha}(t_f - \tau) - \boldsymbol{\alpha}(t_f)] + e\mathbf{A}(t_f) \tag{3.15}$$

Since we are using numerical methods and working on a grid it's possible that we won't find harmonic trajectories with n as an integer only. We expand our search to include trajectories where n is almost an integer, i.e. $n = 1 \pm 0.01, 2 \pm 0.01, 3 \pm 0.01...$ Taking the real part of the position yields this formulation for the trajectory:

$$\mathbf{r}_n(t') \equiv \mathrm{Re}[\mathbf{r}(t') - \mathbf{r}(t_f - \tau)] = \frac{\hbar}{m}(t' - t_f)\,\mathrm{Re}[\mathbf{q}(t_f - \tau, t_f)] + \boldsymbol{\alpha}(t') - \boldsymbol{\alpha}(t_f) \tag{3.16}$$

We repeat these calculations and analysis for corotating and counter-rotating fields of different intensity ratios. We present here results for two counter-rotating fields and one corotating field in depth by plotting the associated electric field, trajectories, and $\boldsymbol{\alpha}(t)$ in sections 3.2.2.1 and 3.2.2.2. Furthermore, we vary the intensity ratio and consider

sets of fields with constant total intensity or constant total U_p. Within these sets we plot the predicted cut-off as a function of the intensity ratio in section 3.2.2.3.

3.2.2 Results for Circular $\omega - 2\omega$ Field Mixing

We present two counter-rotating fields and a corotating field. The data is presented in Figs. 3.2-3.13 in this order: 3D parametric plot of the electric field with time as a geometric axis, trajectories for this field, parametric plot of the electric field with a dot marking the value of $\mathbf{E}(t_f)$ for each trajectory, and a parametric plot of $\boldsymbol{\alpha}(t)$ with a dot marking the value of $\boldsymbol{\alpha}(t_f)$ for each trajectory. The dots are the same color as the trajectory they are associated with, and the harmonic value of the emitted photon is written next to the dot. Afterward, in Figs. 3.14 and 3.15, we present plots showing the maximum harmonic versus intensity ratios for sets of counter-rotating fields. This is a semi-classical method to maximize the cut-off for field mixing.

With finding physical intuition in mind we can ask more specific questions: When during the field cycle does HHG occur? What does an improbable HHG trajectory look like? These questions are explored within the relevant subsection.

To identify the intensity ratio we define a new set of parameters: $I_1 = (i/6)I_{total}$ and $I_2 = (j/6)I_{total}$ such that the total intensity $I_1 + I_2 = I_{total}$ is constant. The next examples have circularly polarized fields with total intensity $I = I_{total} = 10^{14}\frac{W}{cm^2}$

3.2.2.1 Circular Counter-Rotating Fields

Counter-rotating fields offer the most promise for HHG with $\omega-2\omega$ field mixing. The case of equal intensity counter-rotating $\omega - 2\omega$ fields have been investigated experimentally in Ref. [21] and found that the electric field with $i/6 + j/6 = 3/6 + 3/6$ does generate harmonics. For the case of counter-rotating fields we investigate the question, **when during the field cycle does HHG occur?** By plotting the recombination time on the parametric electric field plot we know when the trajectories end and when harmonics are emitted; however, the data does not show a clear region of either the electric field plot or the quiver motion plot where recombination was concentrated. (See Fig. 3.4 and Fig. 3.8 for electric field plots and 3.5 and Fig. 3.9 for the quiver motion plots.) The harmonic energy level doesn't seem to be correlated to the recombination time, either. **What does a typical HHG trajectory look like?** The quiver radius is defined for an electron placed in the field with no initial momentum. Trajectories with small momenta at the tunnel exit, t_i, are likely have a path that looks similar to $\boldsymbol{\alpha}(t)$. Consider the trajectory plots Fig. 3.3 and Fig. 3.7 to note the trajectories that look like the quiver

motion. A trajectory with small momentum at t_i implies the field requires more time to accelerate the electron and return it to the nucleus; therefore, trajectories that are similar to $\boldsymbol{\alpha}(t)$ have longer excursion times. Milosevic et al. [2] suggest that a long excursion time implies that the associated trajectory is unlikely. This statement could be understood by considering the electron as a wave packet which exhibits dispersion properties. The longer time the electron spends in the continuum corresponds to less chance of recombination since the particle isn't localized. If we accept that longer excursion times mean less probability then the more a trajectory looks like $\boldsymbol{\alpha}(t)$, the less likely it is to cause HHG. To confirm or disprove this hypothesis we would need to do a full calculation of the electric dipole moment. We plan to calculate this quantity in the future and connect it to the trajectories.

The partial intensities for the next set are $i/6+j/6 = 3/6+3/6$, which implies $3/6*I = I_1$, $3/6 * I = I_2$.

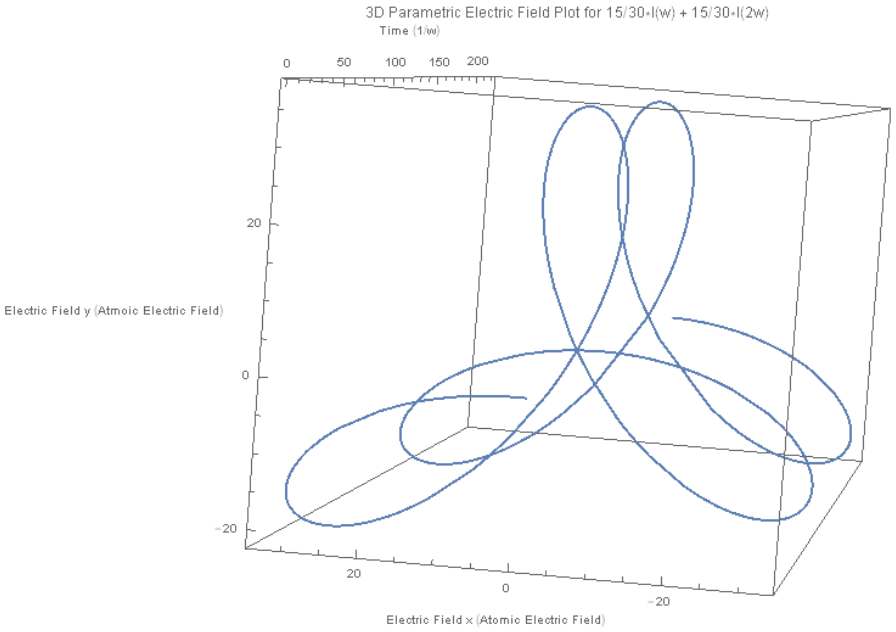

FIGURE 3.2: 3D Parametric Electric Field for counter-rotating $i/6 + j/6 = 3/6 + 3/6$. Time, in field cycles, is plotted into the page. The magnitude of the electric field in the x and y directions is plotted on the plane parallel to the page in atomic units. (Multiplied by 500 for scale.)

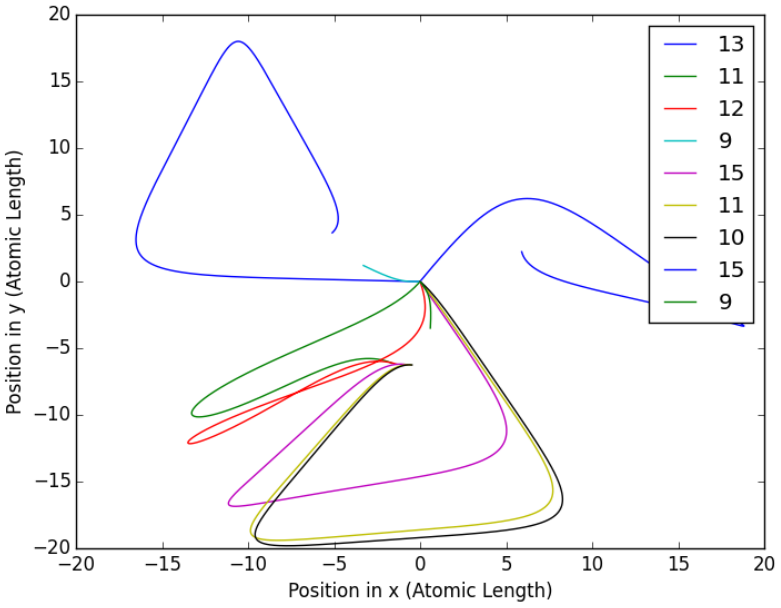

FIGURE 3.3: Trajectories given a driving field like 3.2 with $i/6 + j/6 = 3/6 + 3/6$. The axes are in atomic units of length. The electrons all tunnel exit away from the origin then follow a colored trajectory towards the origin where they emit a high harmonic photon. The emitted photon's harmonic order is shown in the legend.

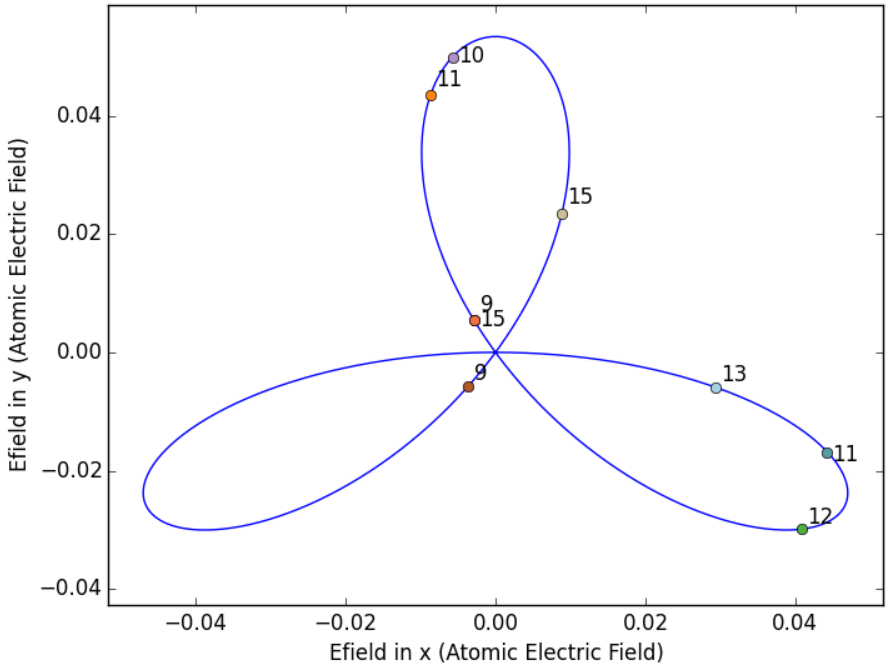

FIGURE 3.4: Parametric Electric Field for counter-rotating $i/6 + j/6 = 3/6 + 3/6$. The axes are in units of atomic electric field. Notice the dots are associated to the recombination times for each trajectory in 3.3

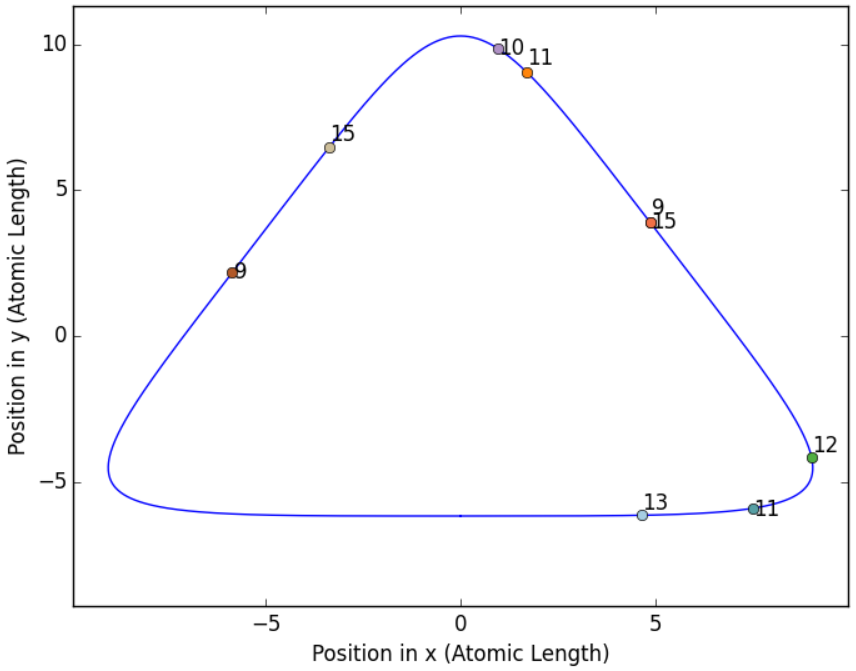

FIGURE 3.5: Parametric $\boldsymbol{\alpha}(t)$ for counter-rotating $i/6 + j/6 = 3/6 + 3/6$. The axes are in atomic units of length. This is the quiver motion plotted in time. Notice the dots are associated to the recombination times for each trajectory in 3.3

The partial intensities for the next set are $i/6+j/6 = 1/6+5/6$, which implies $1/6*I = I_1$, $5/6 * I = I_2$.

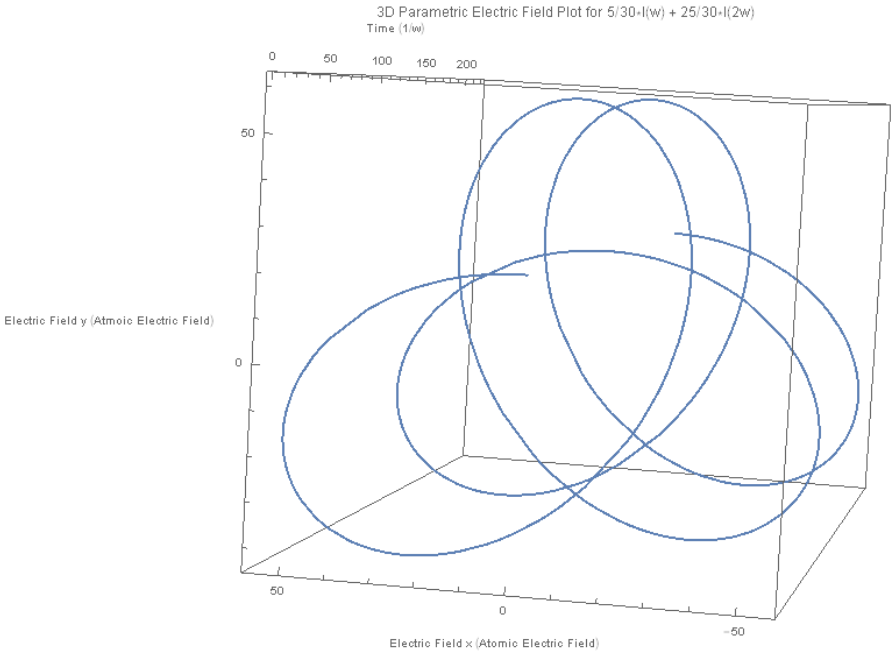

FIGURE 3.6: 3D Parametric Electric Field for counter-rotating $i/6 + j/6 = 1/6 + 5/6$. Time, in field cycles, is plotted into the page. The magnitude of the electric field in the x and y directions is plotted on the plane parallel to the page in atomic units. (Multiplied by 500 for scale.)

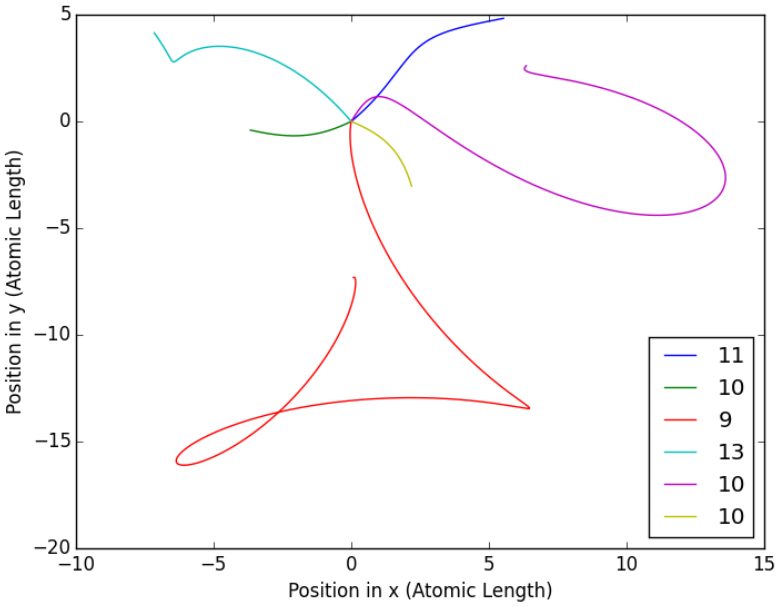

FIGURE 3.7: Trajectories given a driving field like 3.6 with $i/6 + j/6 = 1/6 + 5/6$. The axes are in atomic units of length. The electrons all tunnel exit away from the origin then follow a colored trajectory towards the origin where they emit a high harmonic photon. The emitted photon's harmonic order is shown in the legend.

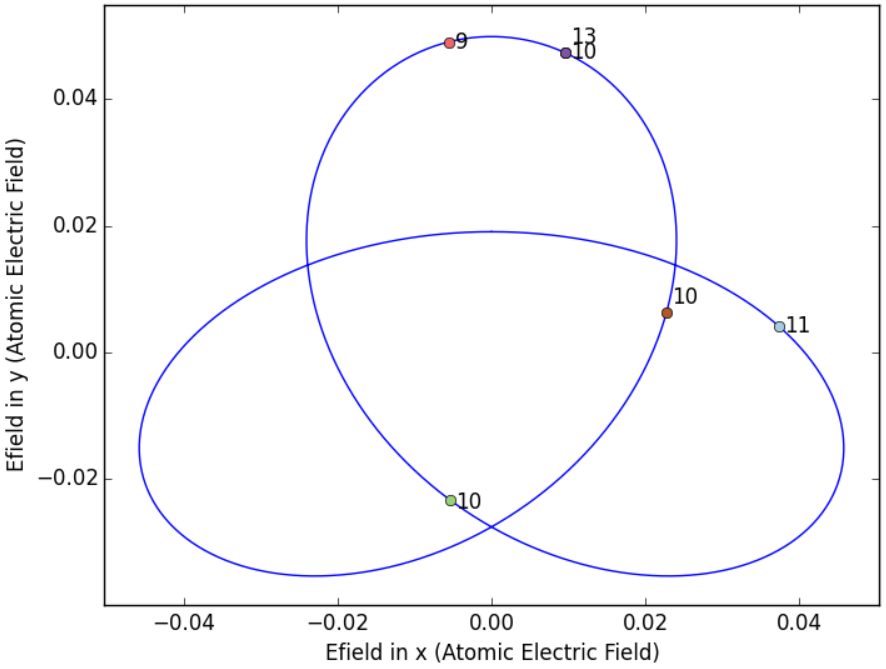

FIGURE 3.8: Parametric Electric Field for counter-rotating $i/6 + j/6 = 1/6 + 5/6$. The axes are in units of atomic electric field. Notice the dots are associated to the recombination times for each trajectory in 3.7

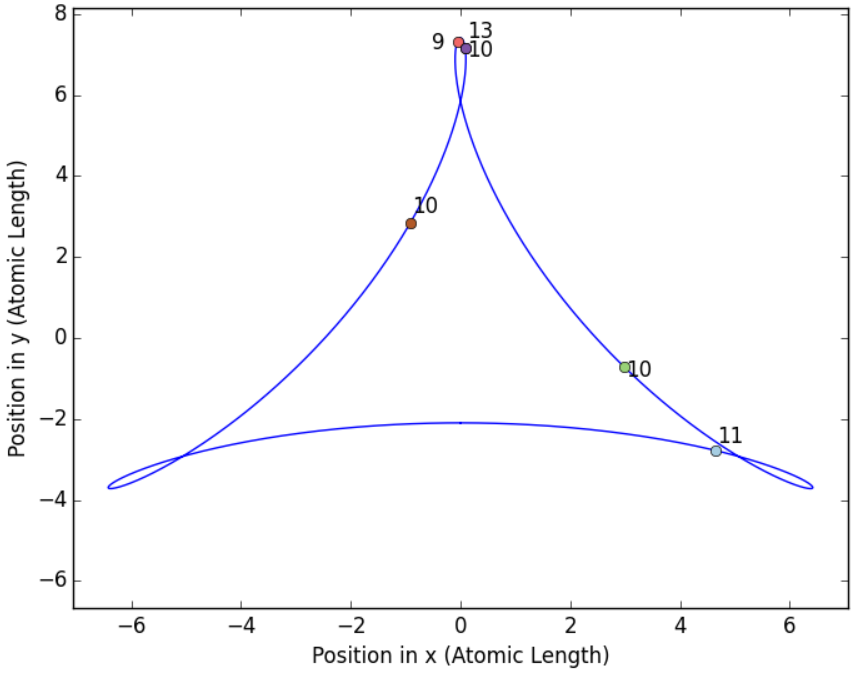

FIGURE 3.9: Parametric $\boldsymbol{\alpha}(t)$ for counter-rotating $i/6 + j/6 = 1/6 + 5/6$. The axes are in atomic units of length. This is the quiver motion plotted in time. Notice the dots are associated to the recombination times for each trajectory in 3.7

3.2.2.2 Circular Corotating Fields

Corotating fields with $i/6 + j/6 = 3/6 + 3/6$ were investigated experimentally in Ref. [21] and it was concluded they do not produce high harmonics. Although the other field combinations were not tested directly in this experiment, it seems likely that no corotating field will generate harmonics. With that in mind we as the question, **when during the field cycle does HHG occur?** Despite the evidence against HHG in this context, let us consider that our trajectories are possible harmonics, in this case there is some amount of grouping in the quiver motion and electric field in the smaller loop, which can be seen in Fig. 3.13 and Fig. 3.12. If we consider Fig. 3.10 we notice that the electric field traces out the small loop for a significant amount of the period, so an evenly distributed set of data points would appear concentrated in the smaller loop as well. Let us now ask the question **What does a typical HHG trajectory look like?** If we consider the trajectories in Fig. 3.11 we notice they require very long tunnel exits to form closed trajectories, and if harmonics are not generated with this system then such long tunnel exits are not very likely. We can support the argument against long distance tunnel exits by considering tunneling through any barrier. The wavefunction within a long classically forbidden region must be exponentially decaying, so the probability of finding the electron tunneling decreases exponentially with distance from the nucleus.

The partial intensities for the next set are $i/6+j/6 = 1/6+5/6$, which implies $1/6*I = I_1$, $5/6 * I = I_2$.

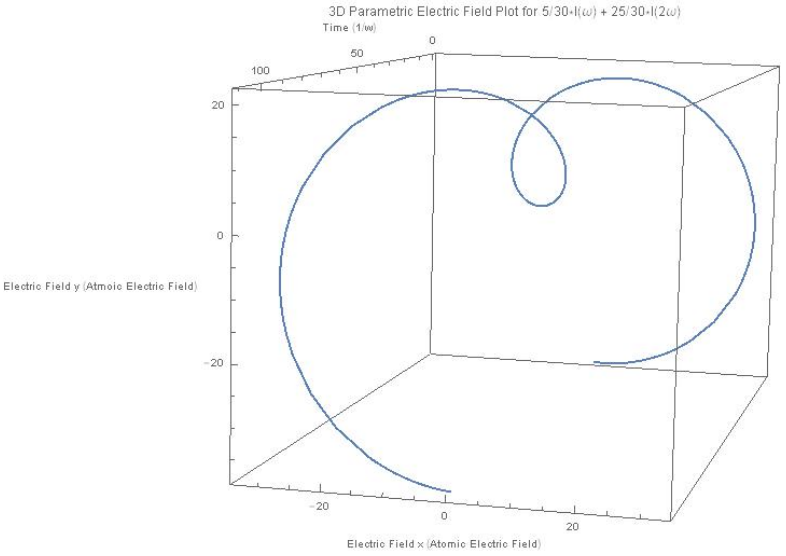

FIGURE 3.10: 3D Parametric Electric Field for corotating $i/6+j/6 = 1/6+5/6$. Time, in field cycles, is plotted into the page. The magnitude of the electric field in the x and y directions is plotted on the plane parallel to the page in atomic units. (Multiplied by 500 for scale.)

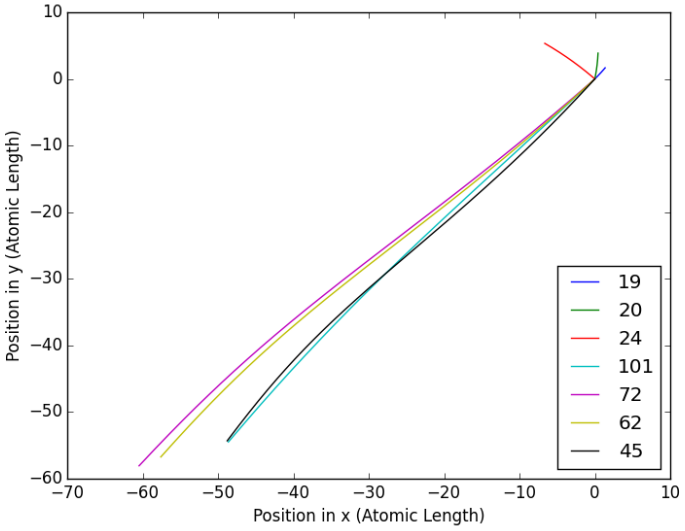

FIGURE 3.11: Trajectories given a driving field like 3.10 with $i/6+j/6 = 1/6+5/6$. The axes are in atomic units of length. The electrons all tunnel exit away from the origin then follow a colored trajectory towards the origin where they emit a high harmonic photon. The emitted photon's harmonic order is shown in the legend.

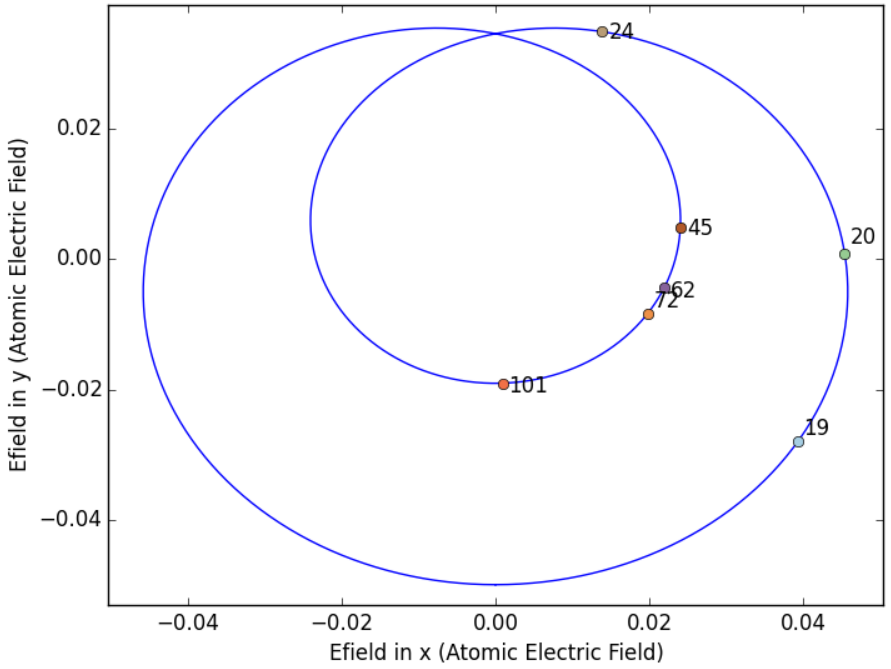

FIGURE 3.12: Parametric Electric Field for corotating $i/6+j/6 = 1/6+5/6$. The axes are in units of atomic electric field. Notice the dots are associated to the recombination times for each trajectory in 3.11

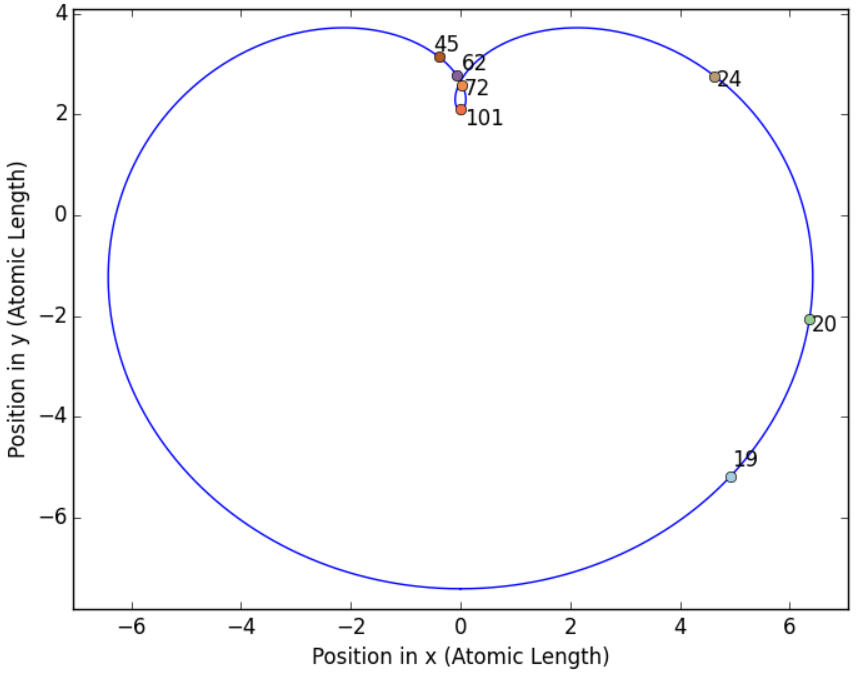

FIGURE 3.13: Parametric $\boldsymbol{\alpha}(t)$ for corotating $i/6 + j/6 = 1/6 + 5/6$. The axes are in atomic units of length. This is the quiver motion plotted in time. Notice the dots are associated to the recombination times for each trajectory in 3.11

3.2.2.3 Semi-classical Cut-Off

In this section we determine the maximum harmonic generated, also known as the cut-off, given a particular combination of intensities using our classical trajectory analysis. We only consider counter-rotating fields. We vary the intensity ratio in 31 steps starting with all of the intensity distributed to the 2ω frequency field then distributing more intensity to the ω field. We redefine i and j such that $i/30 + j/30$ implies $i/30 * I = I_1$ and $j/30 * I = I_2$ with $I_1 + I_2 = I_{total} = I$ constant. Milosevic et al. present a cut-off law for fields with equal intensity distribution.

$$n_{max}\hbar\omega = \frac{1}{\sqrt{2}}3.17U_p + 1.2|E_0| \tag{3.17}$$

We only expect agreement for one point on the plot, but the cut-off law is plotted anyway to see how well it models other intensity distributions. For each set of field components we find the trajectory which leads to the highest harmonic. The results are plotted in Figs. 3.14 and 3.15.

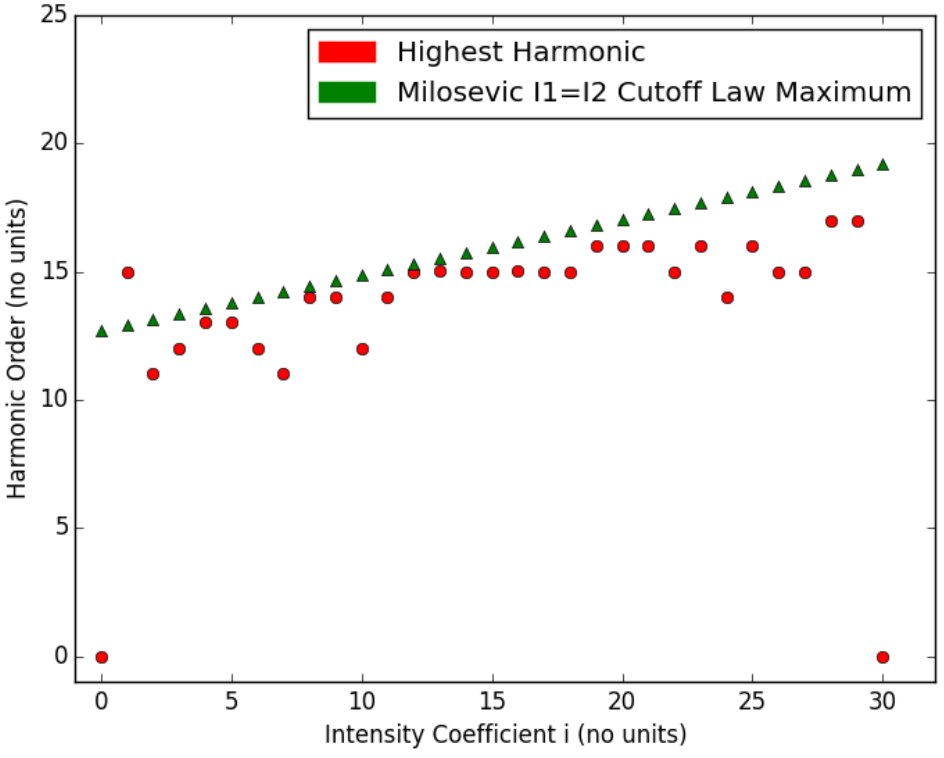

FIGURE 3.14: The counter-rotating fields are held at a constant intensity of $10^{14}\frac{W}{cm^2}$. At the far left, all the intensity is distributed to the 2ω frequency field. As i increases, the intensity of the ω field increases and the intensity of the 2ω field decreases. Notice no harmonics are generated when $i = 0$ and $i = 30$ because the net field is circularly polarized at those ratios.

We can repeat the process but this time using a constant total ponderomotive energy. Recall $U_p = e^2E_1^2/(4m\omega^2) + e^2E_2^2/(16m\omega^2) = U_{p1} + U_{p2}$. Redefine i and j such that $i/30 + j/30$ implies $i/30 * U_p = U_{p1}$ and $j/30 * U_p = U_{p2}$ while holding U_p constant. We plot Milosevic's cut-off law, but we only expect agreement on a single point of the graph where the intensity is equally distributed to the fields.

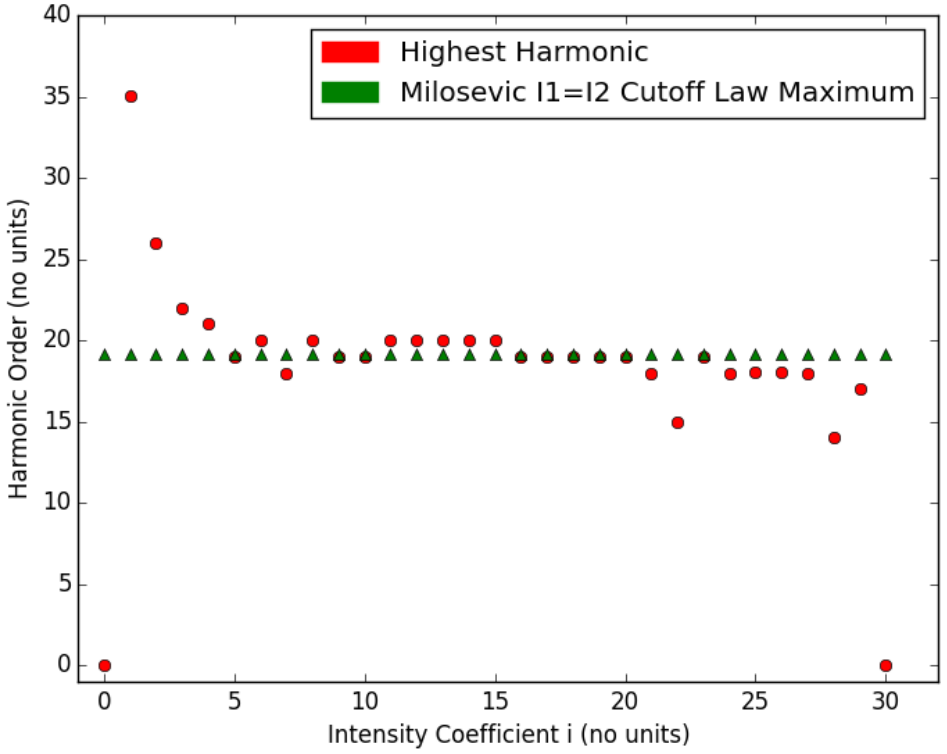

FIGURE 3.15: The counter-rotating fields are held at a constant $U_p = 0.22$ atomic units of energy. The intensities range from $4 \times 10^{14} - 1 \times 10^{14} \frac{W}{cm^2}$ starting at $i = 0$ and approaching $i = 30$. At the far left, all the ponderomotive energy is distributed to the 2ω frequency field. As i increases, the ponderomotive energy of the ω field increases and the ponderomotive energy of the 2ω field decreases. Notice no harmonics are generated when $i = 0$ and $i = 30$ because the net field is circularly polarized at those ratios.

In the constant intensity plot, Fig. 3.14, we see relatively good agreement in the region where the intensity is equally distributed between the fields; however, in the region with high ω intensity our calculations drop off. In the constant ponderomotive energy plot, Fig. 3.15, there is very close agreement with equal distribution of ponderomotive energy. In the intense 2ω region we predict much higher harmonics, in contrast to the intense ω region where we predict lower harmonics. In general, we found the harmonic cut-off in good agreement with predictions by Milosevic's law.

Chapter 4

Conclusion

We presented a comprehensive overview of the process of HHG, starting by introducing some background information like polarization, quantum and classical perspectives on light, and an introduction to the strong field. Next, we covered quantum and semi-classical descriptions of HHG for linear driving fields, then we expanded them to the $\omega-2\omega$ field mixing case. We presented the methods used to generate the trajectories and other relevant plots for linear polarization and circularly polarized $\omega - 2\omega$ field mixing. Finally, we included a maximum harmonic versus intensity ratio plot for maximizing the cut-off using semi-classical predictions.

Our goal was to extend and support our physical intuition for the process of HHG given $\omega - 2\omega$ field mixing. This research represents the foundation of that search. Extending physical intuition is not a precisely defined concept, but by generalizing what we have learned from our results we can explain what happens to HHG electrons in the presence of intense fields. We characterized the driving electric field with a parametric plot with time on a geometric axis to clarify the time evolution of the field. We noted the value of the electric field at the recombination time on the electric field plot so we could see trends of when recombination occurred during the field cycle. We repeated the process with the quiver radius, $\boldsymbol{\alpha}(t)$. We noticed from these parametric plots that the bottom left half of the cycle does not generally contain recombination events using our search parameters.

Each of these recombination events has a harmonic and trajectory associated to it, which we found by means of the saddle points for the quasi-classical action. The technique allows us to calculate closed trajectories for arbitrary intensity distributions of mixed elliptically polarized $\omega - 2\omega$ fields. We qualitatively characterized the probability of a particular trajectory based on its similarity to the quiver radius, noting that a trajectory similar to quiver radius is unlikely to contribute to the overall spectrum. The highest

harmonics we calculated conformed to the prediction from Milosevic's cut-off Eqn. 3.17 in regions of nearly equal intensity distribution between the ω and 2ω fields. At first, we expected our method to find harmonics higher than are probable, which means that the cut-off would be reported to be higher; however, searching for the lowest value of imaginary tunneling time selects for relatively probable trajectories. It is possible to find approximate trajectories by simulation if one randomly guesses initial parameters and allows the system to evolve in time; a similar technique to what we used for the linear case. Our method is superior because it selects for trajectories that obey conservation laws and are thus more likely.

We succeeded in characterizing the difference in trajectories from the corotating and counter-rotating cases. We noted the incredibly long tunnel exit required for the corotating case, which does not lead to HHG, compared with the counter-rotating case which has probable closed trajectories. It is important to note that paths of these sets of trajectories are unintuitive and none of them are similar to published linear trajectories. The search for these trajectories was non-trivial and will be useful in the future to experimentalists and theorists alike.

We successfully used classical methods to analyze High Harmonic Generation with a focus on $\omega - 2\omega$ field mixing. The code used to find these trajectories is adaptable and can prove useful in further pursuits. The method of searching for saddle points is not limited to $\omega - 2\omega$ field mixing and can be extended to driving fields of arbitrary frequency ratios as well as pulsed driving fields. The flexibility of this method allows us to use this code to support ongoing experiments at the Joint Institute for Laboratory Astrophysics (JILA). Although the project was studied and motivated in the context of HHG, this method could be used for studying other strong field effects such as Above Threshold Ionization and Double Ionization since these processes can be described by an electron accelerated in a strong driving field.

4.1 Further Research

There are two primary steps moving forward. Determine how probable a particular trajectory is, and find the rest of the trajectories. Determining the probability for a trajectory could be achieved by calculating the spectrum in combination with Amosov-Delone-Krainov theory (ADK) [7]. ADK helps us determine the ionization rate for a certain electric field value. The spectrum contains information about the length of the plateau, the amplitude of the harmonics present, and at which frequency the cut-off lies. The spectrum would help to determine the probability of a particular trajectory. This is important in $\omega - 2\omega$ field mixing because we allow a tunnel exit away from the origin.

For example, a particular trajectory might yield a high harmonic, but the trajectory requires a very long range tunnel exit. Our intuition tells us that tunneling such a long distance is unlikely, so this trajectory wouldn't contribute to the harmonic spectrum. However, the only way of knowing whether a trajectory contributes is by knowing the spectrum itself. If the harmonic isn't present in the spectrum then that trajectory is unlikely, or even impossible. The usefulness of knowing the spectrum is exemplified by the corotating case. Circularly polarized corotating $\omega - 2\omega$ fields with equal intensity distributions do not generate any harmonics [21]. Though they were not presented, we found trajectories for this case of field mixing. If we hadn't known the spectrum we could only assume that the trajectories were unlikely because they required incredibly long tunnel exit length. The spectrum would allow us to determine the accuracy of the plots for the cut-off versus the intensity ratio. (Figs. 3.15 and 3.14) We could compare our semi-classical predictions to the accurate cut-off determined by the spectrum.

When it comes to finding trajectories, we determined that the search should be expanded. In the expanded search we should generate a grid of taus ranging from zero to the period of the driving field, then search over two periods for t_f. Rather than searching for tau in a box in the complex plane, we should include imaginary values that are higher than the length of one period of the driving field. Learning about what happens in these cases should give us a broader look at the possible trajectories, including the higher harmonics.

Bibliography

[1] P. B. Corkum. Plasma perspective on strong field multiphoton ionization. *Phys. Rev. Lett.*, 71(13), September 1993. URL http://journals.aps.org/prl/abstract/10.1103/PhysRevLett.71.1994.

[2] Dejan B. Milosevic, Wilhelm Becker, and Richard Kopold. Generation of circularly polarized high-order harmonics by two-color coplanar field mixing. *Phys. Rev. A*, 61(6), May 2000. URL http://journals.aps.org/pra/abstract/10.1103/PhysRevA.61.063403.

[3] David J. Griffiths. *Introduction to Electrodynamics (4th Edition)*. Addison-Wesley, 2012.

[4] Albert Einstein. Concerning an heuristic point of view toward the emission and transformation of light. *Annalen der Physik*, 17(132):132–148, 1905. URL http://einsteinpapers.press.princeton.edu/vol2-trans/100.

[5] C.R. Nave. Hyperphys, 2014. URL http://hyperphysics.phy-astr.gsu.edu/hbase/hph.html.

[6] G. Farkas and C. Toth. Proposal for attosecond light pulse generation using laser induced multiple-harmonic conversion processes in rare gases. *Phys. Lett. A*, 168(447), 1992. URL http://loasis.lbl.gov/assets/files/1-s2.0-037596019290534S-main.pdf.

[7] Carlos Hernandez Garcia. *Coherent attosecond light sources based on high-order harmonic generation: influence of the propagation effects*. PhD thesis, Universidad de Salamanca, January 2013.

[8] P. Agostini, F. Fabre, G. Mainfray, G. Petite, and N. Rahman. Free-free transitions following six-photon ionization of xenon atoms. *Phys. Rev. Lett.*, 42(1127), 1979.

[9] A. L'Huillier, L. A. Lompre, G. Mainfray, and C. Manus. Multiply charged ions formed by multiphoton absorption processes in the continuum. *Phys. Rev. Lett.*, 48 (1814), 1982.

[10] L. A. Lompre, G. Mainfray, C. Manus, and J. Thebault. Multiphoton ionization of rare gases by a tunable- wavelength 30-psec laser pulse at 1.06 μm. *Phys. Rev. A*, 15(1604), 1977.

[11] Tom Allison with UC Berkeley. High harmonic generation, 2004. URL http://budker.berkeley.edu/Physics208/harmonicpresent.pdf.

[12] Eadweard Muybridge. The horse in motion, 2002. URL http://hdl.loc.gov/loc.pnp/cph.3a45870.

[13] Ofer Kfir, Patrik Grychtol, Emrah Turgut, Ronny Knut, Dmitriy Zusin, Dimitar Popmintchev, Tenio Popmintchev, Hans Nembach, Justin M. Shaw, Avner Fleischer, Henry Kapteyn, Margaret Murnane, and Oren Cohen. Generation of bright phase-matched circularly-polarized extreme ultraviolet high harmonics. *Nat. Photonics*, 9:99–105, 2015.

[14] University of California Irvine. An introduction to circular dichroism spectroscopy. URL http://www.chem.uci.edu/~dmitryf/manuals/Fundamentals/CD%20spectroscopy.pdf.

[15] Daniel E. Adams, Christopher S. Wood, Margaret M. Murnane, and Henry C. Kapteyn. Tabletop high harmonics illuminate the nano-world. *Laser Focus World*, 2015.

[16] M. Lewenstein, Ph. Balcou, M. Yu. Ivanov, Anne L'Huillier, and P. B. Corkum. Intense few-cycle laser fields: Frontiers of nonlinear optics. *Phys. Rev. A*, 49(2117), 1994. URL http://dx.doi.org/10.1103/PhysRevA.49.2117.

[17] Saddle point method of asymptotic expansion. URL http://bolvan.ph.utexas.edu/~vadim/Classes/2011f/saddle.pdf.

[18] M V Fedoryuk. Saddle point method, 2001. URL https://www.encyclopediaofmath.org//index.php?title=Saddle_point_method.

[19] T. Popmintchev, M. Chen, P. Arpin, M. M. Murnane, and H. C. Kapteyn. The attosecond nonlinear optics of bright coherent x-ray generation. *Nature Photonics*, 4:822–832, November 2010. URL http://www.nature.com/nphoton/journal/v4/n12/abs/nphoton.2010.256.html.

[20] Alexandra S. Landsman and Ursula Keller. Attosecond science and the tunnelling time problem. *Physics Reports*, 547:1–24, 2015. URL http://www.sciencedirect.com/science/article/pii/S0370157314003159.

[21] Maithreyi Gopalakrishnan. *Tomographic Reconstructions of Photoelectron Distributions from Strong-Field Ionization in Two-Color Circularly Polarized Laser Fields.* B.S. Thesis, University of Colorado, March 2015.